

HYDROGENATION OF NANODIAMOND SURFACES: STRUCTURE AND EFFECTS ON CRYSTALLINE STABILITY

S. P. RUSSO,* A. S. BARNARD and I. K. SNOOK

Department of Applied Physics, Royal Melbourne Institute of Technology University,

GPO Box 2476V Melbourne, 3001 Australia

Presented are results of our ab initio study of the surface reconstruction and relaxation of (100) surfaces on bulk and nanocrystalline diamond. We have used a density functional theory (DFT) within the generalized-gradient approximation (GGA) via the parallel computer version of the Vienna ab initio simulation package (VASP), to consider dehydrogenated and hydrogenated surfaces. Edges and corners of nanocrystals offer a new challenge in the determination of surface structure. We have applied the methodology for stepped diamond (100) surfaces to this problem, and consider it useful in describing nanodiamond edges and corners to first approximation. Our results also indicate that dimer lengths and atomic layer depths of the $C(100)(2 \times 1)$ and $C(100)(2 \times 1)$: H nanodiamond surfaces differ slightly from those of bulk diamond. The effects of these differences on crystalline stability are discussed, with the intension of offering a better understanding of the effects of nanodiamond surfaces on the stability of diamondoid nanostructures.

1. Introduction

The study of diamond surfaces has received considerable attention over recent decades, prompted mainly by advances in the growth of diamond films using chemical vapor deposition (CVD) methods. More recently, diamond(carbon)-based materials have been proposed as the optimal choice for nanomechanical designs due to their high elastic modulus and strength-to-weight ratio. An important aspect of simulating nanodiamond structures is to correctly model their surfaces. Clean¹⁻⁹ and hydrogen-passivated⁴⁻³⁰ C(100) bulk diamond surfaces have been the topic of many investigations using a variety of experimental and theoretical methods.

Presented in this report is a density functional theory (DFT) study of the energetics and relative stability of selected nanocrystalline diamond structures using the Vienna *ab initio* simulation package (VASP).^{31,32} We used ultrasoft, gradient-corrected Vanderbilt type pseudopotentials³³ as supplied by G. Kresse and J. Hafner,³⁴ and the valence orbitals

are expanded on a plane-wave basis up to a kinetic energy cutoff of 290.00 eV. These have been extensively tested for carbon and have been shown to give results in excellent agreement with all-electron ab initio methods, 34,25 and good agreement with experiment. 35

The nanocrystal relaxations were performed in the framework of DFT within the generalized-gradient approximation (GGA), with the exchange-correlation functional of Perdew and Wang. ³⁶ Using this method the calculated lattice parameter for bulk diamond of 3.561 Å, the sp³ bond length of 1.541 Å and the band gap E_g of 5.46 eV are all in excellent agreement with the experimental values of 3.566 Å, ³⁷ 1.544 Å³⁷ and 5.48 eV, ³⁸ respectively.

DFT studies of the $C(100)(2 \times 1)$ -reconstructed and stepped (100) surfaces have been performed by Furthmüller $et~al.^{28}$ and Alfonso $et~al.^{39}$ respectively. In this study we also determine the relaxation of bulk diamond surfaces as a check of our computational methodology, and as a prelude to the relaxation of nanodiamond surfaces.

^{*}Author to whom correspondence should be addressed.

2. Surface Relaxations

In order to fully relax the surface of bulk diamond slabs and nanodiamonds, both the ions and supercell volume were relaxed. 25,28 Thus, both the symmetry and the lattice parameter of the nanocrystals were free to alter, resulting in expansions or contractions of the entire structures. Each ionic step consisted of a minimum of three electronic steps, followed by calculation of the Hellmann–Feynman forces. The relaxations were performed for a minimum of 20 ionic steps, consisting of approximately 50–60 electronic steps initially, and converging to a minimum of three electronic steps for the final ions steps.

2.1. Relaxation of bulk diamond surfaces

In this study both the dehydrogenated $C(100)(2 \times 1)$ and monohydrogenated $C(100)(2 \times 1)$: H surface have been considered, using an infinite diamond slab consisting of 144 carbon atoms with periodic boundary conditions (PBCs) in the x and y directions, and the 5 Å of vacuum space in the z direction forming two (100) surfaces. It has been shown by others that this amount of vacuum space is sufficient.^{4,28}

The monohydrogenated diamond slab was generated by saturating each surface of a dehydrogenated 144-carbon-atom slab with 12 hydrogen atoms, giving a total 24 hydrogen atoms. The dehydrogenated and monohydrogenated surfaces are then treated separately, and compared with the results of other

Table 1. Comparison of average bulk C(100) reconstructed surfaces with reported theory and experimental values.

Bulk Surface Comparison						
	This Study	DFT^{28}	DF-TB ⁴	SW^3		
C(100)						
d_{11} (Å)	1.385 ± 0.003	1.37	1.40	1.68 ± 0.05		
d_{12} (Å)	1.517 ± 0.006	1.50	1.52	1.56 ± 0.04		
Z_{12} (Å)	0.68 ± 0.08	0.67	_	0.86 ± 0.06		
Z_{23} (Å)	0.91 ± 0.08	0.79	_	0.97 ± 0.06		
C(100):H				$\mathrm{Expt.}^{29}$		
d_{11} (Å)	1.632 ± 0.008	1.61	1.67	1.60 ± 0.05		
d_{12} (Å)	1.545 ± 0.005	1.53	1.59	-		
Z_{12} (Å)	0.81 ± 0.06	0.80	_	0.81 ± 0.03		
Z_{23} (Å)	0.91 ± 0.09	0.79	-	0.90 ± 0.06		

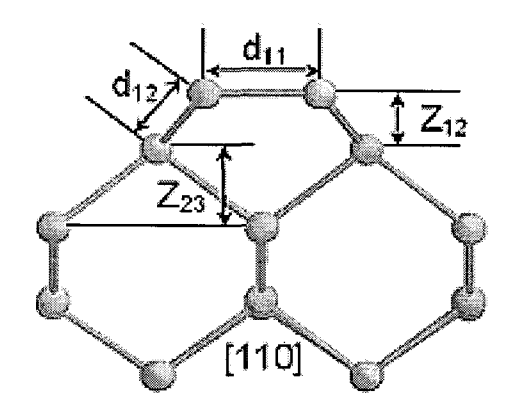


Fig. 1. $C(100)(2 \times 1)$ dimer from the [110] direction.

theoretical and experimental research groups. This comparison is given in Table 1, with the nomenclature as defined in Fig. 1.

The $C(100)(2 \times 1)$ surface may be described in further detail by considering difference between symmetric and asymmetric dimer patterns, as previously done by Frauenheim et al.⁵ and Skokov et al.,²⁷ both using molecular dynamics based on a quantum-mechanically derived semiempirical density functional approach. Our results of such calculations are listed in Table 2. These results show that the primary d_{11} dimer length is slightly larger for the asymmetric zigzag pattern, in line with the findings of Skokov et al. and Frauenheim et al. It is also

Table 2. Surface dimer lengths and atomic layer depths for the symmetric and asymmetric $C(100)(2 \times 1)$ and $C(100)(2 \times 1)$: H bulk diamond surfaces.

Bulk Diamond Surface						
	Symmetric Asymmetric					
	This Study	PM3 ⁶	This Study	PM3 ⁶		
C(100)		-				
$d_{11} \ (ext{Å})$	1.382 ± 0.003	1.53	1.387 ± 0.002	1.57		
$d_{12} \ (ext{Å})$	1.507 ± 0.003	-	1.527 ± 0.006	_		
Z_{12} (Å)	0.69 ± 0.08	_	0.673 ± 0.004	_		
Z_{23} (Å)	0.87 ± 0.08	_	0.946 ± 0.005	_		
C(100):H						
d_{11} (Å)	1.617 ± 0.003	1.66	1.647 ± 0.008	1.71		
$d_{12} \ ({ m \AA})$	1.538 ± 0.005	_	1.553 ± 0.004	_		
Z_{12} (Å)	0.80 ± 0.06	_	0.82 ± 0.003	_		
Z_{23} (Å)	0.91 ± 0.09	_	0.91 ± 0.003	_		

important to note that none of the results here show any dimer buckling, in full agreement with previously reported theoretical, ²⁸ and experimental ⁴⁰ results.

Relaxation of nanodiamond surfaces

In total, four {100} cubic nanodiamonds were constructed, each with two (100) faces and four (110) faces. The (110) surface is considered to be stable (with only a minor relaxation occurring) as it retains the (1×1) surface structure. 11 Therefore all surface reconstructions were confined to the two (100) faces of the nanodiamonds. The two dehydrogenated nanodiamond structures considered here consist of a small 54-atom nanocrystal, with a diameter just over 0.5 nm, and a larger 259-atom nanocrystal, with a diameter just over 1 nm.

The relaxed structures for the dehydrogenated C₅₄ and C₂₅₉ nanodiamonds are given in Fig. 2 and Fig. 3, respectively. The C_{54} and the C_{259} nanodiamonds retained the diamond structure following relaxation; however, inspection of Fig. 2 reveals that the nanocrystal has undergone a type of shearing during this process, resulting in a triclinic (rather than cubic) structure. This will be discussed in more detail later.

The dangling bonds on a C_{54} nanocrystal and a C₂₅₉ nanocrystal were then terminated with hydrogen atoms, forming two (100) and four (110) monohydrogenated surfaces each. The monohydrogenated surfaces were perturbed, to form the (2×1) : H dimer pattern, prior to relaxation to reduce simulation times. The hydrogen terminations then rearranged on the surface, to adopt the equilibrium H-C bond lengths and angles, and the surface dimer lengths and layer depths relaxed.

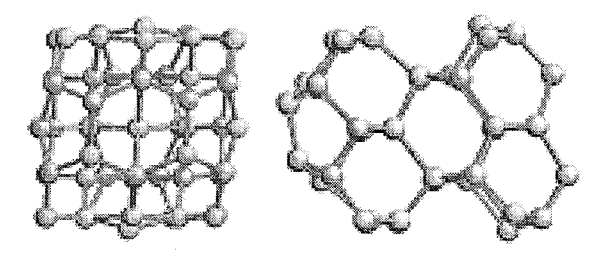
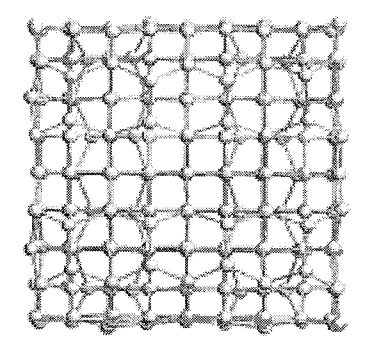


Fig. 2. Relaxed C₅₄ nanocrystal, from the [100] (left) and [110] (right) directions.



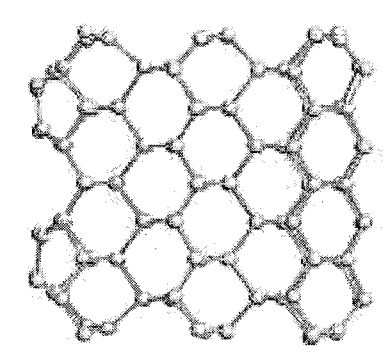


Fig. 3. Relaxed C₂₅₉ nanocrystal, from the [100] (top) and [110] (bottom) directions.

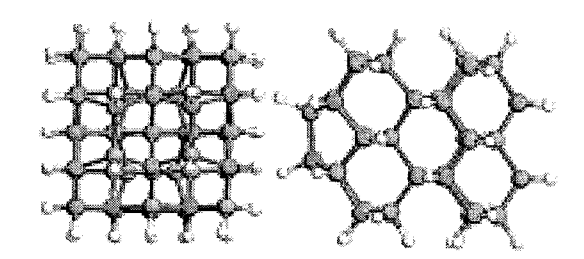
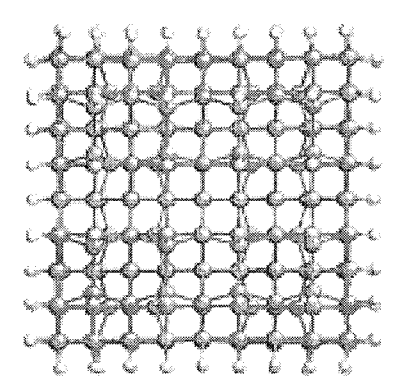


Fig. 4. Relaxed $C_{54}H_{48}$ nanocrystal, from the [100] (left) and [110] (right) directions.

Both the $C_{54}H_{48}$ and the $C_{259}H_{140}$ nanodiamonds retained the diamond structure following relaxation. The relaxed structures for the dehydrogenated dehydrogenated and monohydrogenated nanodiamonds are given in Fig. 4 and Fig. 5, respectively.

The C_{259} and the $C_{259}H_{140}$ nanodiamonds were found to have surface reconstructions and relaxations comparable to bulk diamond. The characterization of the nanodiamond surfaces has been



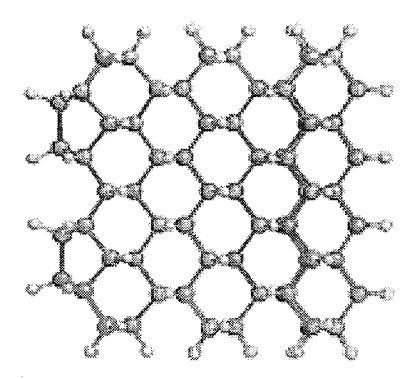


Fig. 5. Relaxed $C_{259}H_{140}$ crystal, from the [100] (top) and [110] (bottom).

performed in detail by considering the difference in d_{11} and d_{12} dimer lengths, and the Z_{12} and Z_{23} layer depths for faces, edges and corners of the nanocrystal. This comparison is given in Table 3.

The d_{11} length for the "center" category is absent from Table 3, as all d_{11} dimers on the $\mathrm{C}_{259}\mathrm{H}_{140}$ nanocrystal fall on an "edge" or a "corner." Since there are only two rows of dimers on the (100) surfaces, the term "edge" has been chosen to describe the nanocrystal edge comprising four dimers (perpendicular to the edge direction) and the term "corner" to describe the nanocrystal edge comprising two dimers (parallel to the edge direction).

Inspection of Table 3 reveals that the surface reconstruction and relaxation varies depending upon the region of the nanocrystal, particularly in the case of the dehydrogenated nanocrystal. In both cases it may be seen that the primary d_{11} dimer length is larger and the first layer relaxation depth Z_{12} is smaller for dimers situated at the nanocrystal corners, than for those situated at the nanocrystal

Table 3. Average surface dimer lengths and upper atomic layer depths for corners, edges and center of the $C(100)(2 \times 1)$ and $C(100)(2 \times 1)$: H surfaces of the $C_{259}H_{140}$ nanodiamonds.

Nanodiamond Surfaces					
	Corner	Edge	Center		
C(100)					
d_{11} (Å)	1.49 ± 0.02	1.39 ± 0.01	_		
d_{12} (Å)	1.42 ± 0.04	1.50 ± 0.02	1.53 ± 0.02		
Z_{12} (Å)	0.65 ± 0.03	0.66 ± 0.05	0.48 ± 0.07		
Z_{23} (Å)	0.86 ± 0.09	0.8 ± 0.12	0.7 ± 0.12		
C(100):H					
d_{11} (Å)	1.64 ± 0.01	1.63 ± 0.01	_		
$d_{12} \ (\mathrm{\AA})$	1.55 ± 0.03	1.53 ± 0.03	1.53 ± 0.03		
Z_{12} (Å)	0.82 ± 0.02	0.83 ± 0.02	0.82 ± 0.04		
Z_{23} (Å)	0.82 ± 0.03	0.85 ± 0.07	0.83 ± 0.07		

edges. The dehydrogenated nanocrystal also has a shortened d_{12} length of 1.42 Å at the corners, and the Z_{12} and Z_{23} layer depths are significantly reduced in the center of the nanocrystal face, being only 0.48 Å and 0.7 Å respectively. This central Z_{12} layer depth represents a reduction of 27% from the average corner/edge result, and a reduction of 46% from the bulk diamond layer spacing. Similarly, the central Z_{23} layer depth of 0.7 Å represents a reduction of 15% from the average corner/edge value and 21% from the bulk diamond layer spacing.

Table 3 shows that monohydrogenation of the nanodiamond surfaces has an important effect on the surface structure. The addition of the hydrogens not only removes the $\rm sp^2$ hybridization at the surface, but also removes much of the variation in surface structure over the (100) faces. The d_{11} and d_{12} dimer lengths and the Z_{12} and Z_{23} layer depths are similar but not identical for the corners, edges and centers of the (100) faces. These results for the dehydrogenated and monohydrogenated nanodiamonds strongly indicate that edges and corners of nanocrystals cannot be ignored during characterization of surface structure.

3. Comparison of Bulk and Nanocrystalline Surface Structure

Ignoring for a moment the variations in surface structure over the (100) faces, the average primary and secondary dimer lengths and average first and second

Table 4. Comparison of average bulk and nanodiamond C(100) reconstructed surfaces. The C_{259} and $C_{259}H_{140}$ nanodiamond results are averaged over the "corner," "edge" and "center" regions.

Surface Comparison				
	Bulk Diamond	Nanodiamond		
C(100)				
d_{11} (Å)	1.385 ± 0.003	1.44 ± 0.06		
d_{12} (Å)	1.517 ± 0.006	1.49 ± 0.08		
Z_{12} (Å)	0.68 ± 0.08	0.59 ± 0.07		
Z_{23} (Å)	0.91 ± 0.08	0.8 ± 0.12		
C(100):H				
d_{11} (Å)	1.632 ± 0.008	1.63 ± 0.02		
d_{12} (Å)	1.545 ± 0.005	1.54 ± 0.04		
Z_{12} (Å)	0.81 ± 0.06	0.82 ± 0.04		
Z_{23} (Å)	0.91 ± 0.09	0.83 ± 0.07		

layer depths for the dehydrogenated and monohydrogenated nanodiamonds have been compared with the corresponding bulk diamond surface results (see Table 4).

The results for the dehydrogenated nanodiamond and bulk diamond surfaces show that the d_{11} dimer length is larger for nanodiamond than for bulk diamond, but the reverse is the case for the d_{12} dimer length. While bulk diamond d_{11} dimer length corresponds to the sp³ double bond length, and the d_{12} dimer length approaches the sp³ single bond length, the nanodiamond d_{11} and d_{12} lengths are both closer to the sp² π -bond length. Both the Z_{12} and Z_{23} layer depths are shallower for the dehydrogenated nanodiamond than bulk diamond, by a significant 0.11 Å. For the monohydrogenated nanocrystal, the d_{11} and d_{12} dimer lengths and the Z_{12} layer depth are equal to the bulk diamond results within errors, with only the Z_{23} layer depth showing a difference.

However, as shown above, edges and corners of the nanodiamonds cannot be ignored. Using the nomenclature of Chadi, 41 single-atom steps on diamond (100) surfaces are denoted as S_A and S_B when the direction of the upper terrace (2×1) dimers are oriented perpendicular to the step edge and parallel to the step edge, respectively. Further, S_B type steps may be denoted as $S_B(n)$ for the non-bonded type, where there are no rebonded atoms on the lower terrace; and $S_B(b)$ for the bonded type, which does have rebonded atoms on the lower terrace. Therefore, if we consider the edges of the nanodiamonds as exaggerated steps, then the structure of the "edges" represents S_A steps, and the "corners" represent $S_B(n)$ steps. Under this assumption, the d_{11} dimer lengths for these step types (given in Table 3) may be compared with the results for stepped bulk diamond (100) surfaces.

Calculations by Alfonso et al. 39 using DFT LDA molecular dynamics determined that for the dehydrogenated surface the symmetric, unbuckled sp² hybridized S_A step had a d_{11} dimer length of 1.37 Å, and the symmetric sp² hybridized S_B step had upper terrace d_{11} dimer lengths of ~ 1.48 Å. In the case of the monohydrogenated stepped surface, the S_A step had a d_{11} dimer length of 1.61 Å. Hence, in this study the calculated d_{11} length for the dehydrogenated nanodiamond edge of 1.39 Å and corner of 1.49 Å are only 0.01 Å greater than the result for the S_A step of 1.37 Å and the $S_B(n)$ step of ~ 1.48 Å. The results for the monohydrogenated nanocrystal edge of 1.63 Å is 0.02 Å greater than the monohydrogenated S_A bulk diamond step of 1.61 Å and are only 0.01 Å greater than results of the hybrid density functional (LDA) tight-binding (DF-TB) molecular dynamics study for the $C(100)(2 \times 1)$: H bulk diamond surface by Skokov et al., 27 where the d_{11} dimer length was found to be 1.62 Å for S_A type steps, and 1.63 Å for S_B type steps.

Implications for crystalline 3.1. stability

The saturation of the nanodiamond surfaces with hydrogen has a great influence on the overall stability of an isolated nanocrystal, and produces a structure of lower energy. The energy per carbon ion has been plotted for each relaxation step for both the 54carbon-atom and the 259-carbon-atom (see Fig. 6) nanodiamonds. In both cases, the energy of the monohydrogenated nanocrystals has been corrected by subtracting the energy of the hydrogen terminations, so that it is possible to compare the energy per carbon atom for the dehydrogenated and monohydrogenated nanocrystals directly. From Fig. 6 we may see that the hydrogenation of the surfaces has resulted in structures with a lower energy.

The lower energy of the hydrogenated nanocrystals in Fig. 6 is entirely due to the passivation of surface bonds, as confirmed by a static single point

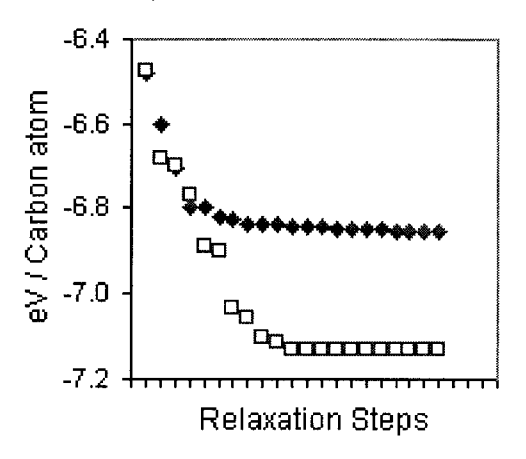


Fig. 6. Energy convergence of C_{259} (\spadesuit) and $C_{259}H_{140}$ (\square) nanocrystals.

energy calculation of the relaxed $C_{54}H_{48}$ nanocrystal with all the hydrogens removed.

Aside from the passivation of the dangling surface bonds, hydrogenation was found to have other effects on the overall stability of the nanocrystals. We have seen that when the corners and edges of the larger nanodiamond are treated as exaggerated steps, the d_{11} dimer lengths may be predicted reasonably from the bulk diamond results, even though the dimer lengths are closer to the length of an sp² π -bond in the case of the dehydrogenated nanocrystal. However, the contraction of the d_{12} dimer length (in conjunction with the extension of the average d_{11} dimer) to the sp² π -bond range at 0 K brings the stability of the diamond structure at the surface at higher temperatures into question. Ab initio molecular dynamics calculations at 300 K are currently underway.

While the dehydrogenated nanodiamond surface structure differs from bulk diamond surfaces in dimer lengths and layer depths, it has been illustrated that hydrogenation of surfaces smears out variations in surface structure over the (100) faces and that the monohydrogenated nanodiamond surface structure more closely mimics the bulk diamond surface structure. Using bulk diamond as a benchmark for structural stability, such improved homogeneity of surface structure must promote stability, as should the adoption of a more bulk-diamond-like surface structure.

Both the $\rm C_{259}$ and $\rm C_{259}H_{140}$ nanodiamonds were also found to exhibit entire nanocrystal relaxations.

The total volume of the C_{259} nanocrystal contracted from 1.29 nm³ upon "cleaving," to approximately 0.95 nm³ following relaxation. The monohydrogenated nanocrystal also contracted, from 1.29 nm³ to approximately 1.06 nm³ (disregarding the hydrogen terminations). This corresponds to a reduction in the lattice constant of 8.2% for the dehydrogenated nanocrystal and 4.7% for the monohydrogenated nanocrystal. However, the contraction of the (100) upper surface layers of the dehydrogenated nanodiamond accounts for a reduction of 0.085 nm³ alone, and thus the full nanocrystal contraction of the dehydrogenated and monohydrogenated nanocrystals differs only by ~ 0.02 nm³ when the (100) surface layer relaxations are ignored.

Finally, as previously mentioned, the C₅₄ nanocrystal underwent a kind of shearing during relaxation, resulting in a structure with triclinic symmetry. Just as full nanocrystal contractions were observed, so this represents an entire nanocrystal relaxation effecting the symmetry; and like the contractions of the nanocrystal volume outlined above, this effect was reduced by hydrogenation of the surfaces (see Figs. 2 and 4).

4. Conclusion

It has been shown that hydrogenation of (100) diamond surfaces on nanocrystalline diamonds serves to produce a more bulk-diamond-like surface structure, and reduces localized structural differences related to nanocrystal corners and edges. Hydrogenation was also found to reduce the shrinking of the nanocrystals upon relaxation, with the full nanocrystal contraction for the monohydrogenated nanodiamond being approximately half that of the dehydrogenated version. Monohydrogenation of the surfaces of the cubic nanodiamond structures investigated here serves not only to passivate the reactive (100) surfaces, but also to stabilize the nanocrystal and enforce a bulk-diamond-like structure and symmetry. Further studies of the type reported here are currently continuing.

Acknowledgments

This project has been supported by the Victorian Partnership for Advanced Computing and the Australian Partnership for Advanced Computing supercomputer center.

References

- B. Weiner, S. Skokov and M. Frenklach, J. Chem. Phys. 102, 13 5486 (1995).
- A. V. Petukhov, A. Fasolino, D. Passerone and F. Ercolessi, *Phys. Stat. Sol. (a)* 174, 19 (2000).
- A. S. Barnard, P. Bath, S. P. Russo and I. K. Snook, Phys. Stat. Sol. (a) (2002) (submitted).
- S. H. Yang, D. A. Drabold and J. B. Adams, *Phys. Rev.* B48(8), 5261 (1993).
- Th. Frauenheim, U. Stephan, P. Blaudeck, D. Porezag, H. G. Busmann, W. Zimmerman-Edling and S. Lauer, *Phys. Rev.* B48(24), 18189 (1993).
- S. Skokov, C. S. Carmer, B. Weiner and M. Frenlach, Phys. Rev. B49(8), 5662 (1994).
- D. Alfonso, D. A. Drabold and S. E. Ulloa, *Phys. Rev.* B51(20), 14669 (1995).
- 8. H. Kawarada, Surf. Sci. 26, 205 (1996).
- S. Hong and M. Y. Chou, Phys. Rev. B55(15), 9975 (1997).
- J. B. Marsh and H. E. Farnsworth, Surf. Sci. 1, 3 (1964).
- P. G. Lurie and J. W. Wilson, Surf. Sci. 65, 453 (1977).
- 12. B. B. Pate, Surf. Sci. 165, 83 (1986).
- 13. B. B. Pate, Surf. Sci 165, 1356 (1990).
- A. V. Hamza, G. D. Kubiak and R. H. Stulen, Surf. Sci. 237, 35 (1990).
- S. P. Mehandra and A. B. Anderson, Surf. Sci. 248, 369 (1991).
- X. M. Zheng and P. V. Smith, Surf. Sci. 256, 1 (1991).
- 17. T. Halicioglu, Diamond Relat. Mater. 1, 963 (1992).
- R. E. Thomas, R. A. Rudder, R. J. Markunas,
 D. Huang and M. Frenklach, J. Chem. Vapour Deposition 1, 6 (1992).
- Y. L. Yang and M. P. d'Everlyn, J. Am. Chem. Soc.
 114, 2796 (1992); Y. L. Yang and M. P. d'Everlyn,
 J. Vac. Sci. Technol. A10, 978 (1992).
- R. E. Thomas, R. A. Rudder and R. J. Markunas, J. Vac. Sci. Technol. A10, 2451 (1992).

- 21. S. T. Lee and G. Apai, Phys. Rev. B48, 2684 (1993).
- T. Aizawa, T. Ando, M. Damo and Y. Sato, Phys. Rev. B48, 18348 (1993).
- H. Sasakż, M. Aokż and H. Kawarada, Diamond Relat. Mater. 2, 1271 (1993).
- B. N. Davidson and W. E. Pickett, Phys. Rev. B49, 11253 (1994).
- J. Furthmüller, J. Hafner and G. Kresse, *Europhys. Lett.* 28, 659 (1994).
- R. E. Stallcup II, A. F. Aviles and J. M. Perez, Appl. Phys. Lett. 66, 18, 2331 (1995).
- S. Skokov, B. Weiner, M. Frenklach, Th. Frauenheim and M. Sternberg, Phys. Rev. B52(7), 5426 (1995).
- J. Furthmüller, J. Hafner and G. Kresse, *Phys. Rev.* B53, 7334 (1996).
- Y. M. Wang, K. W. Wong, S. T. Lee, M. Nishitani-Gamo, I. Sakaguchi, K. P. Loh and T. Ando, *Phys. Rev.* B59(15), 10347 (1999).
- K. Bobrov, G. Comtet, G. Dujardin and L. Hellner, Surf. Sci. 482-485, 437 (2001).
- G. Kresse and J. Hafner, Phys. Rev. B47, RC558 (1993).
- G. Kresse and J. Hafner, Phys. Rev. B54, 11169 (1996).
- 33. D. Vanderbilt, Phys. Rev. B41, 7892 (1990).
- G. Kresse and J. Hafner, J. Phys.: Condens. Matter 6, 8245 (1994).
- G. Kern, J. Hafner and G. Kresse, Surf. Sci. 366, 445 (1996).
- J. Perdew and Y. Wang, Phys. Rev. B45, 13244 (1992).
- H. J. McSkimin and P. Andreatch, J. Appl. Phys. 43, 2944 (1972).
- A. Mainwood, Properties and Growth of Diamond, ed. G. Davies (INSPEC, London, 1993), p. 3.
- 39. D. Alfonso, D. Drabold and S. Ulloa, J. Phys.: Condens. Matter 8, 641 (1996).
- S. Walter, J. Bernhardt, U. Starke, K. Heinz, J. Ristein and L. Ley, J. Phys.: Condens. Matter 14, 3085 (2002).
- 41. D. J. Chadi, Phys. Rev. Lett. 43, 43 (1987).